Available online at www.sciencedirect.com
SCIENCE DIRECT®
Journal of Solid State Chemistry 174 (2003) 471–481
JOURNAL OF SOLID STATE CHEMISTRY
http://elsevier.com/locate/jssc

Crystallographic, electronic and magnetic studies of $Ce_4Ni_6Al_{23}$: a new ternary intermetallic compound in the cerium–nickel–aluminum phase diagram

Delphine Gout, Evan Benbow, Olivier Gourdon, and Gordon J. Miller*

Department of Chemistry, Iowa State University, Gilman Hall, Iowa 50011-3111, Ames, IA, USA

Received 31 July 2002; received in revised form 7 November 2002; accepted 17 November 2002

Abstract

The Al-rich portion of the ternary Ce–Ni–Al has been investigated and a new ternary phase of composition $Ce_4Ni_6Al_{23}$ has been found. This compound crystallizes in the monoclinic space group $C2/m$ with the cell parameters $a = 16.042(8)$, $b = 4.140(4)$, $c = 18.380(8)$ Å and $\beta = 113.24(5)^\circ$. The structure has been determined by single crystal X-ray diffraction. The local environment of Ni and Ce is close to what is observed in the $CeNi_2Al_5$ and $CeNiAl_4$ structures. Band structure calculations, using the tight-binding–linear muffin-tin orbital–atomic-spheres approximation (TB-LMTO-ASA) method, have been performed to understand the electronic structure of $Ce_4Ni_6Al_{23}$ and the results are discussed in connection with those two other Ce–Ni–Al intermetallic compounds, which possess heavy-fermion behavior. Magnetic and heat capacity measurements have also been measured to analyze the low-temperature magnetic behavior of this new compound.

Keywords: Intermetallic compounds; Aluminum; Cerium; Nickel; Ab initio band structure calculations

1. Introduction

The Ce–Ni–Al ternary phase diagram is rich with various phases such as CeNiAl [1,2], $CeNi_2Al_3$, $Ce_2Ni_5Al_5$, $CeNi_2Al_7$, $CeNi_2Al_5$ and $CeNiAl_4$ [2]. Our interest was to investigate new compounds in the Al-rich portion of this ternary diagram to explore the Ni–Al networks that form with larger rare-earth metals to search for new polar intermetallic compounds. We are also interested in the orbital and magnetic coupling between the "diluted" rare-earth atoms and the metallic network. In this region three compounds, close in stoichiometry, are already known: $CeNi_2Al_5$, $CeNiAl_4$ and $CeNi_2Al_7$ [2]. However, the structure of $CeNi_2Al_7$ is still unknown. During our investigation in this Al-rich region, a new ternary compound, which is formulated as $Ce_4Ni_6Al_{23}$, was synthesized. This compound crystallizes in the monoclinic space group $C2/m$ with the cell parameters $a = 16.042(8)$, $b = 4.140(4)$, $c = 18.380(8)$ Å and $\beta = 113.24(5)^\circ$. The structure was determined by single crystal X-ray diffraction. The local environments of the Ce and Ni are close to what is observed in $CeNiAl_4$ [2,3].

Among all these intermetallic compounds in the ternary Ce–Ni–Al system, $CeNi_2Al_5$ and $CeNiAl_4$ have attracted much attention due to their exceptional electric and magnetic properties [3–9]. Indeed, $CeNi_2Al_5$ is a famous magnetic, heavy-fermion compound with a magnetic transition at 2.6 K and $CeNiAl_4$ is a non-magnetic, heavy-fermion compound ($T_k \approx 67$ K). Since there are structural similarities between $Ce_4Ni_6Al_{23}$ and $CeNiAl_4$, interesting magnetic properties could be expected for the former compound which we report herein. Therefore, magnetic, resistance and heat capacity measurements have been carried out to analyze the magnetic behavior of this new compound. Thereafter, tight-binding–linear muffin-tin orbital–atomic-spheres approximation (TB-LMTO-ASA) calculations were performed on $Ce_4Ni_6Al_{23}$ and $CeNiAl_4$ to understand their electronic structures and interpret the magnetic measurements.

*Corresponding author. Fax: +515-294-0105.
E-mail address: gmiller@iastate.edu (G.J. Miller).

0022-4596/03/$ - see front matter © 2003 Elsevier Science (USA). All rights reserved.
doi:10.1016/S0022-4596(02)00167-6

2. Experimental

2.1. Synthesis and analyses

Because various phases coexist during growth from the liquidus close to this composition (Fig. 1), preparation of our samples demanded close attention. The compound was prepared from cerium (ingots, Ames laboratory, 99.99%) nickel (powder, Johnson Matthey, 99.997%) and aluminum (pellets, Aldrich, 99.99%) in the molar ratio Ce:Ni:Al = 4:6:23. The elements were arc melted under high purity argon on a water-cooled copper hearth. The weight loss during melting was less than 0.2%. An X-ray powder diffraction pattern was collected on a Scintag XDS2000 diffractometer to check the purity of our sample. The alloy was annealed at 1073 K in evacuated silica tubes for 10 days to improve the crystallinity and to obtain a sufficient size for single crystal measurements. After cooling from 1073 to 673 K for 2 days and, thereafter, a natural cooling to room temperature of the closed furnace, the final product was obtained. These crystals are stable upon exposure to air and water. A microprobe analysis by energy dispersive X-ray spectroscopy (EDS) performed on a Hitachi S-2460N ESEM gave the chemical formula $Ce_{4.0(1)}Ni_{6.1(1)}Al_{22.3(3)}$. To obtain the quantitative values, Al, Ni and CeO_2 were used as standards.

2.2. Physical property measurements

The temperature dependence of the resistance was measured on a single block by a conventional four-probe AC method in the temperature range 1.8–300 K starting from 1.8 K (PPMS Instrument). Measurements of magnetization and magnetic susceptibility were carried out using a vibrating sample magnetometer in the temperature range 1.8–300 K (MPMS-5 SQUID Magnetometer, Quantum Design, Inc.). The magnetization measurements were done in the range of field from 1 to 100 kOe. The specific heat was measured by a standard adiabatic method in the temperature range from 1.8 to 20 K.

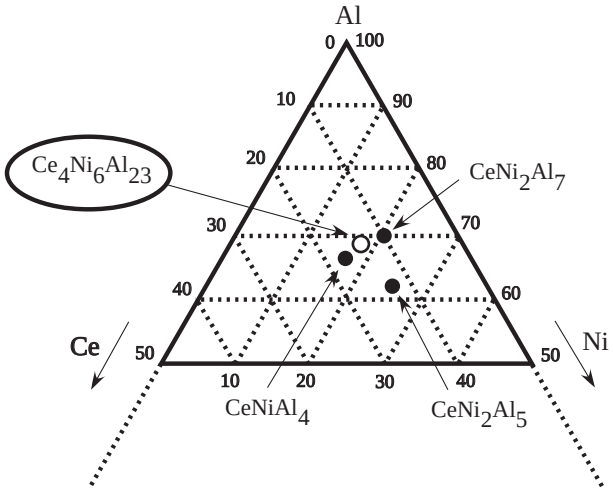

Fig. 1. Phase diagram of Ce–Ni–Al system at 1073 K in the Al-rich portion.

2.3. Structure determination

Diffracted intensities were collected at room temperature with a *P*4 single-crystal diffractometer (Siemens, Karlsruhe, Germany). The entire set of reflections was consistent with monoclinic symmetry and could be indexed by a *C*-centered lattice ($a \approx 16.0$ Å, $b \approx 4.1$ Å, $c \approx 18.4$ Å and $\beta \approx 113.2^\circ$). The intensities of the reflections were adjusted for Lorentz-polarization and corrected for absorption via a Gaussian analytical method, and the crystal shape and dimensions were optimized with the *Stoe* X-Shape program [10] on the basis of equivalent reflections. All data treatments, refinement and Fourier syntheses were carried out with the JANA2000 program package [11]. The reflection sets were averaged according to the $2/m$ point group, yielding internal *R* values less than 6% for observed reflections ($I > 2\sigma(I)$) (see Table 1 for more information). All refinements were performed on F^2 with all reflections included, but the residual *R* factors are reported for observed reflections only.

A structural model for $Ce_4Ni_6Al_{23}$ was established using direct methods (SIR97 program [12]). A first series of refinement cycles with isotropic displacement parameters yielded an *R*-value of 5.78% (50 parameters). Introduction of anisotropic displacement parameters and of a secondary extinction coefficient (type I) led to $R = 4.14\%$ for 192 parameters. At this point, the difference Fourier analysis showed positive and negative electronic residues in the vicinity of the two rare-earth sites ($\approx 3\,e^-\,Å^{-3}$). A nonharmonic development of these two sites up to the fourth order features no higher electronic residues than $1.92\,e^-\,Å^{-3}$ and no lower electronic residues than $-1.69\,e^-\,Å^{-3}$. The refinement converges to an *R*-value of 3.52% for 132 parameters. However, the third order terms were not significant and so only the even orders were kept (second and fourth orders) in the final refinement, which gave the same *R*-value of 3.52% for only 122 parameters. Atomic positions are listed in Table 2. Bond distance ranges are listed in Table 3.

3. Structural discussion

$Ce_4Ni_6Al_{23}$ crystallizes in a new structure type and exhibits a three-dimensional structural arrangement illustrated in Fig. 2. According to the (010) projection in Fig. 2, which includes the unit cell of $Ce_4Ni_6Al_{23}$, we identify two different motifs building up the structure of

Table 1
Crystallographic and experimental data

	Physical and crystallographic data
Formula	$Ce_4Ni_6Al_{23}$
Molecular weight ($g\,mol^{-1}$)	1533.21
Crystal system	Monoclinic
Space group	$C2/m$ (No. 12)
Z	2
Cell parameters	$a = 16.042(8)$ Å
	$b = 4.140(4)$ Å
	$c = 18.380(8)$ Å
	$\beta = 113.24(5)^\circ$
	$V = 1121(1)$ Å^3
Density calc. ($g\,cm^{-3}$)	4.537
	Data collection
Temperature	293 K
Radiation	$\lambda_{MoK-L2,3} = 0.71069$ Å
Diffractometer	Siemens P4
Angular range $2\theta(^\circ)$	0–52
$h\,k\,l$ range	$-19 \leqslant h \leqslant 18$
	$0 \leqslant k \leqslant 5$
	$0 \leqslant l \leqslant 22$
	Data reduction
Linear absorption coefficient (cm^{-1})	137.42
Absorption correction	Analytical
Total recorded reflections	2578
Observed reflections ($I > 2\sigma(I)$)	1175
Rint (%)	9.68
	Refinement
Refinement	F^2
Weighting scheme	$W = 1/(\sigma^2\lvert F_o\rvert + (0.01 * 0.01\lvert F_o\rvert)^2)$
No. of refined parameters	122
Refinement results	$R(\%) = 3.51$
	$R_w(\%) = 8.46$
	GOF = 2.31
Residual electronic density	$[-1.64, +1.91]e^-$ Å^{-3}

$Ce_4Ni_6Al_{23}$. These two slabs have the formulations $Ce_3Ni_2Al_{12}$ and $CeNi_4Al_{11}$. Such a description suggests that $Ce_4Ni_6Al_{23}$ could be an intergrowth compound of other structure types. However, to our knowledge, none of these slabs is known separately. It seems that the stability is created by the "juxtaposition" of these two slabs.

One simple way to explain this structure is to describe the local environment of the two Ce sites and the three Ni sites (see Fig. 3) and to understand how they connect together. The Ni environments are slightly distorted trigonal prisms: these are made by six Al for Ni(2), whereas they are built with four Al and two Ce for Ni(1) and Ni(3). All of these trigonal prisms are capped in the equatorial plane by Al. However, the $[Ni(1)Al_4Ce_2]$ trigonal prism is tetracapped, whereas the $[Ni(2)Al_6]$ and $[Ni(3)Al_4Ce_2]$ trigonal prisms are tricapped (see Fig. 3). The environment observed for the Ni(3) site is similar to what is found in $CeNiAl_4$ [6]. (The coordination environment for Ni(1) can also be described as a distorted cube of Al atoms with two face-capping Ce atoms). The ranges of Ni–Al distances (between 2.370(2) Å and 2.561(2) Å for Ni(1), 2.507(2) Å and 2.804(2) Å for Ni(2), 2.343(3) Å and 2.538(2) Å for Ni(3)) and Ni–Ce distances (between 3.290(3) Å and 3.307(3) Å) are in good agreement with those observed for $CeNiAl_4$ [6] and $CeNi_2Al_5$ [5]. The two Ce sites, also shown in Fig. 3, are rather similar with just slight differences in interatomic distances between both sites. These Ce atoms are surrounded by 13 Al and two Ni atoms with a shape that is close to a cuboctahedron.

Along the b-axis the Ce(1) polyhedra and Ce(2) polyhedra share pentagonal faces (4Al + 1Ni) with their analogues to form quasi-infinite chains $^1_\infty[Ce(1)Ni_2Al_9]$ and $^1_\infty[Ce(2)Ni_2Al_9]$, which connect together by Al–Ce

Table 2
Fractional atomic coordinates and equivalent isotropic atomic displacement parameter of $Ce_4Ni_6Al_{23}$.

Atom	Wyckoff position	x	y	z	ADP_{eq}(Å^2)
Ce1	4i	0.26445(3)	0	−0.28226(5)	1.10(6)
Ce2	4i	0.57002(3)	0	−0.09317(5)	1.09(6)
Ni1	4i	0.30989(8)	0	−0.56644(7)	1.12(3)
Ni2	4i	−0.00741(8)	0	−0.63292(7)	1.22(3)
Ni3	4i	−0.22619(8)	0	−0.89737(7)	1.17(3)
Al1	4i	0.4312(2)	0	−0.4400(2)	1.41(8)
Al2	4i	0.1247(2)	1/2	0.0956(2)	1.46(8)
Al3	4i	−0.0317(2)	−1/2	−0.2826(2)	1.44(8)
Al4	2a	0	0	0	1.4(1)
Al5	4i	0.4177(2)	−1/2	−0.1879(2)	1.44(8)
Al6	4i	0.2040(2)	0	−0.9784(2)	1.27(7)
Al7	4i	−0.0899(2)	0	−0.7778(2)	1.33(8)
Al8	4i	0.3565(2)	1/2	−0.3588(2)	1.26(7)
Al9	4i	−0.2220(2)	1/2	−0.8235(2)	1.36(8)
Al10	4i	−0.1075(2)	1/2	−0.6591(2)	1.27(7)
Al11	4i	0.2548(2)	0	−0.4549(2)	1.27(8)
Al12	4i	−0.0898(2)	0	−0.5476(2)	1.40(8)

Table 3
Bond distances ranges (Å) in $Ce_4Ni_6Al_{23}$

Ce1–Ni	3.290(1)	Ce2–Ni	3.307(1)		
Al	3.094(2)–3.391(3)	Al	3.107(3)–3.334(3)		
Ni1–Al	2.370(2)–2.561(2)	Ni2–Al	2.416(4)–3.059(3)	Ni3–Al	2.343(3)–2.538(1)
Al–Al	2.617(4)–2.898(4)				

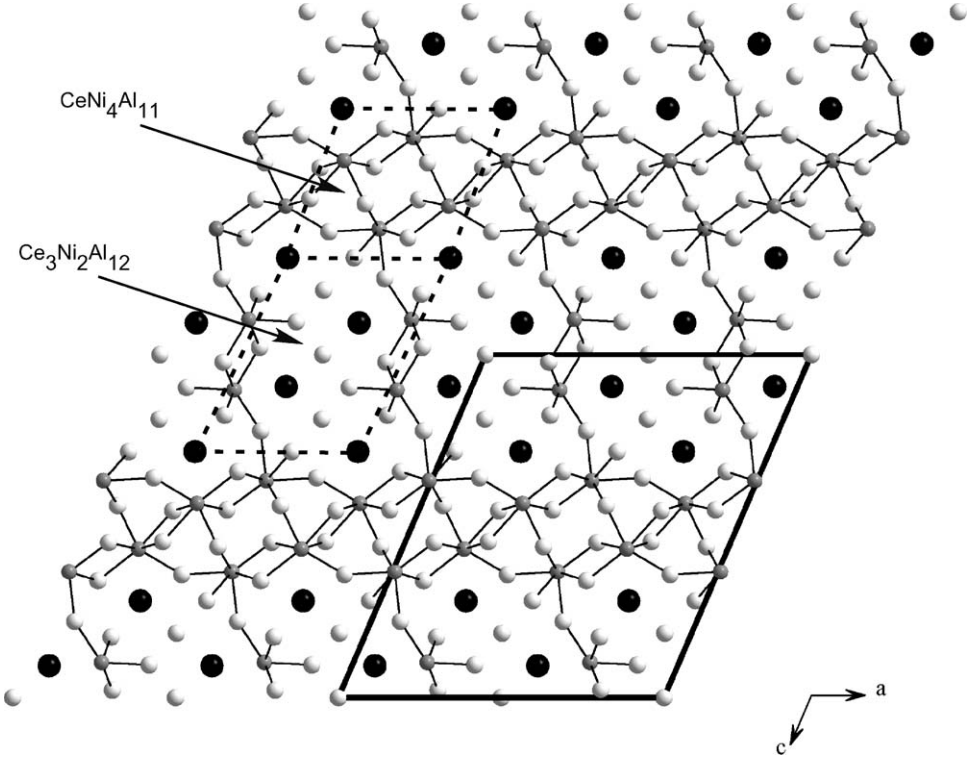

Fig. 2. View along the *b*-axis of the unit cell of $Ce_4Ni_6Al_{23}$. In dashed lines are represented two hypothetic subunit cells ($Ce_3Ni_2Al_{12}$ and $CeNi_4Al_{11}$) as discussed in the text. Gray, black and white circles represents Ni, Ce and Al, respectively.

edges to form sheets in the (*a*,*b*) plane (see Fig. 4). The space between these planes is filled by Ni atoms.

4. Physical property measurements

Heavy-fermion compounds containing Ce or other rare-earth elements are well suited to study the role of strong electron correlations in metals. $Ce_4Ni_6Al_{23}$ is a new example for understanding hybridization between the 4*f* states and the network-derived valence 3*p* and 3*d* states. Since the structural environments in $Ce_4Ni_6Al_{23}$ and $CeNiAl_4$ are similar, some interesting physical properties can be expected for the new compound, $Ce_4Ni_6Al_{23}$. The temperature dependence of the resistance, *R*, for $Ce_4Ni_6Al_{23}$ is shown in Fig. 5. The resistance is nearly temperature independent above 120 K, and rapidly decreases as the temperature is lowered below 120 K, which suggests some strong electronic correlations. These correlations were also observed in $CeNiAl_4$ below 120 K by Mizushima et al. [3].

Fig. 6 shows the temperature dependences of the susceptibility χ and the reciprocal susceptibility $1/\chi$ in the temperature range 1.8–300 K. Above 100 K, the susceptibility follows the Curie–Weiss law with effective moment $\mu_{eff} = 2.60\,\mu_B$, which is close to the free Ce^{3+} ion value of $2.54\,\mu_B$. The Ce ions of this compound above 100 K are in a trivalent state as observed for $CeNiAl_4$, considering that the Ni ions do not contribute to the effective moment. Below 100 K, the reciprocal susceptibility $1/\chi$ slightly increases then rapidly decreases and deviates from the Curie–Weiss law. The paramagnetic Curie temperature extrapolated for $Ce_4Ni_6Al_{23}$ from the high temperature data is $\theta_p = -225$ K. This large negative paramagnetic Curie temperature is in good agreement with strong electronic correlations.

The specific heat was also measured on a 0.20 g sample of $Ce_4Ni_6Al_{23}$. The temperature dependent heat

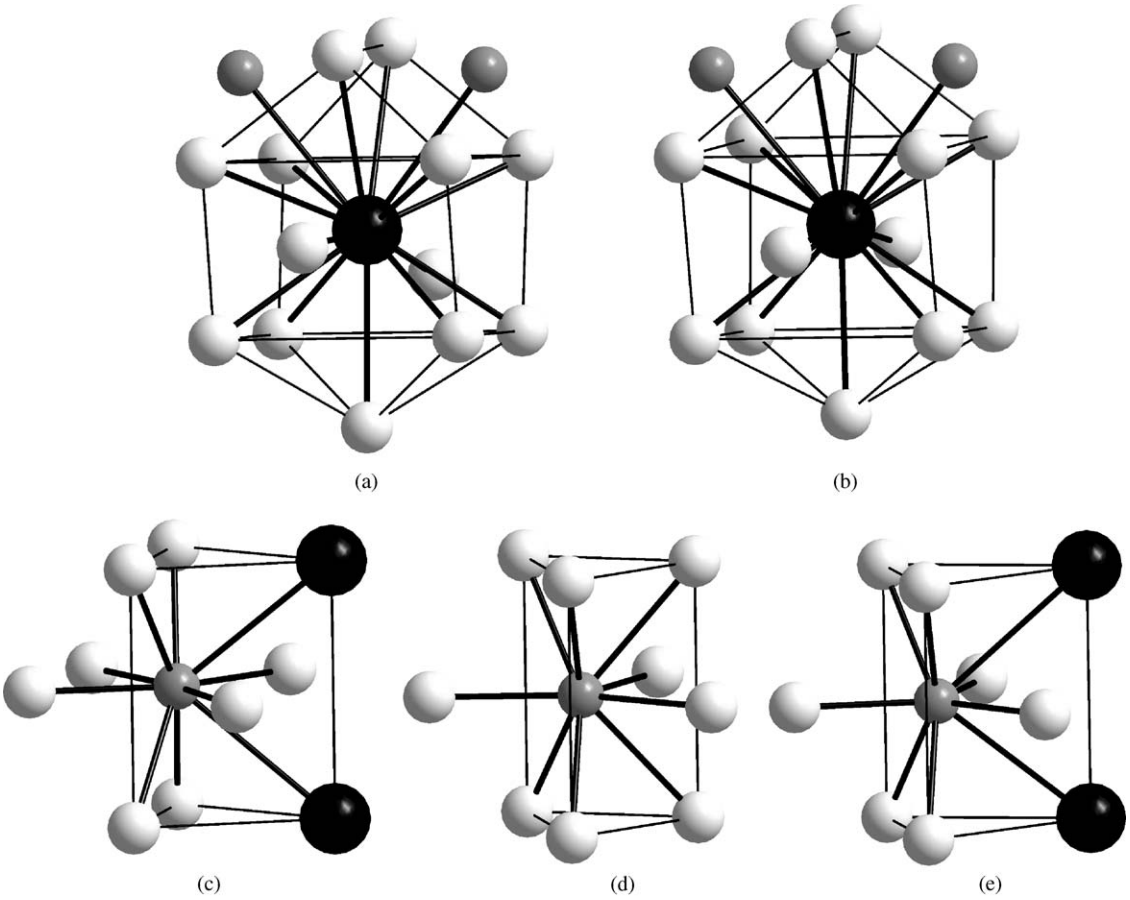

Fig. 3. Representation of the different local environments (a) for Ce1 and (b) for Ce2 and (c) for Ni1, (d) for Ni2 and (e) for Ni3.

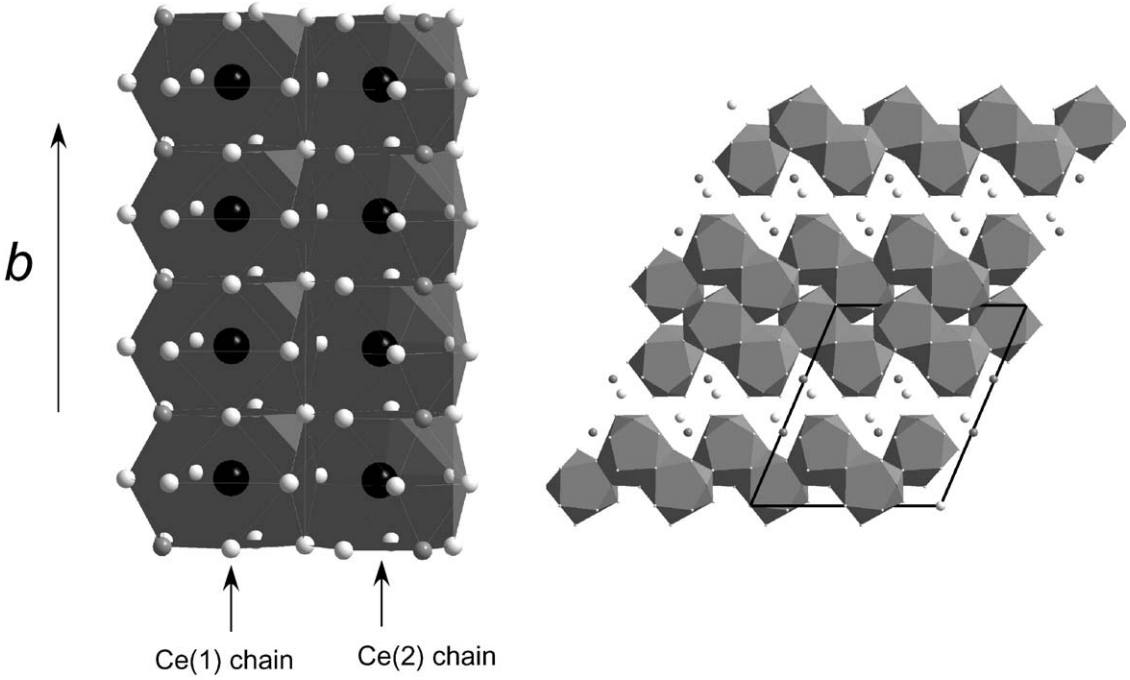

Fig. 4. Representation of the different connections between (a) Ce1 and Ce2 polyhedra to form chains.

capacity, shown in Fig. 7, follows a T-law above 7 K. Below 7 K (Fig. 7 in the inserted graph) two anomalies are observed around 3 and 6 K. These anomalies were already suspected from the susceptibility measurements. Mizushima et al. also observed an anomaly in this temperature range for $CeNiAl_4$, which was explained by a valence fluctuation for $CeNiAl_4$. A plot of C_p/T versus T^2 in the temperature range 0–10 K (Fig. 7) extrapolated to 0 K allows an estimate of γ_0 in $Ce_4Ni_6Al_{23}$, which gives ca. 130 mJ/mol K^2. γ_0 is 175 mJ/mol K^2 for $CeNiAl_4$ [3]. γ_0 not only provides information about the density of states at the Fermi level for a metal, it is also a good parameter to evaluate the strength of electronic correlations. In a classical metal γ_0 is typically rather small ($\sim$10 mJ/mol K^2), while for a heavy-fermion system it is usually equal to at least 400 mJ/mol K^2. In $Ce_4Ni_6Al_{23}$ the intermediate γ_0 value indicates that strong electronic correlations are present even if we cannot consider this compound among the strongest heavy-fermion compounds. Integration of the C_p/T versus T curve between 0 and 6 K gives us an

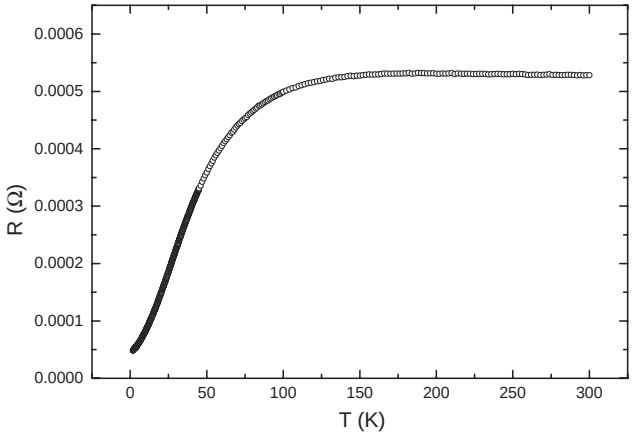

Fig. 5. Temperature dependence of the resistance of a bulk of $Ce_4Ni_6Al_{23}$ sample between 0 and 300 K.

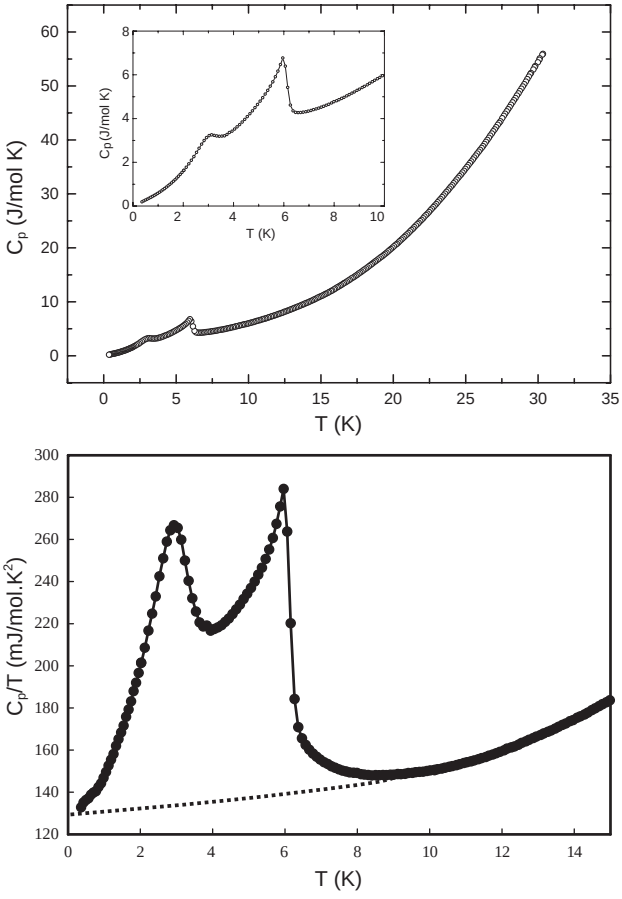

Fig. 7. The temperature dependence of the entropy S for $Ce_4Ni_6Al_{23}$. Two anomalies are observed at 3 and 6 K. Specific heat divided by the temperature C/T for $Ce_4Ni_6Al_{23}$, plotted as a function of T.

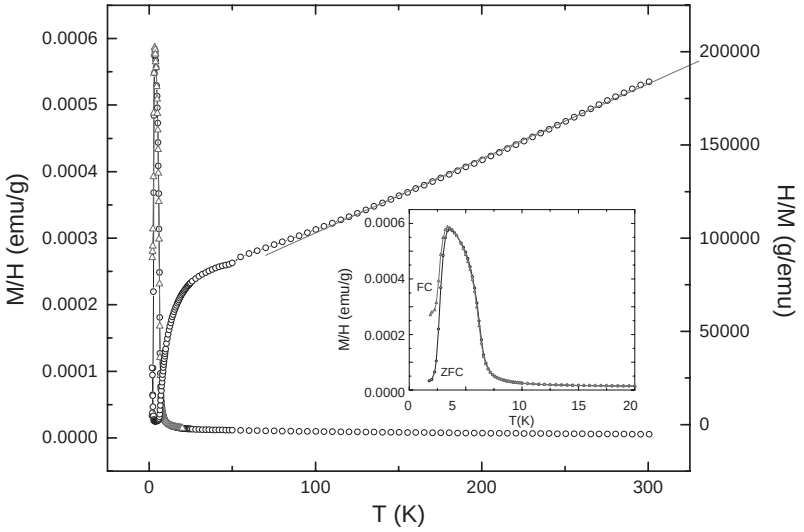

Fig. 6. Temperature dependence of the susceptibility χ and the reciprocal susceptibility $1/\chi$ of a bulk of $Ce_4Ni_6Al_{23}$ sample between 0 and 300 K for a field of 1 kG.

estimation of the entropy of the "magnetic part" with respect to the electronic and lattice part. This result is approximately 1500 mJ/mol K, which is rather low compared to what we might theoretically expect for Ce^{3+}, i.e., $S = R \ln 2 = 4800$ mJ/mol K.

Since the physical property characteristics of $Ce_4Ni_6Al_{23}$ and $CeNiAl_4$ are very close to each other, except for some different anomalies, a comparative analysis of both electronic structures could be helpful to understand their magnetic behaviors.

5. Electronic structure calculations

Band structure calculations on $Ce_4Ni_6Al_{23}$ and $CeNiAl_4$ have been performed to shed some light on the origin of the magnetic behavior of these compounds, in particular, to examine the possible interaction between the Ce-4*f* orbitals and the conduction bands.

5.1. Computational details

TB-LMTO electronic band structure calculations were carried out on $Ce_4Ni_6Al_{23}$ and $CeNiAl_4$ in the atomic sphere approximation using the LMTO47 program [13]. Exchange and correlation were treated in a local spin density approximation [14]. All relativistic effects except spin–orbit coupling were taken into account using a scalar relativistic approximation [15].

In the atomic sphere approximation, space is filled with small overlapping Wigner–Seitz (WS) atomic spheres. The symmetry of the potential is considered to be spherical inside each WS sphere, and a combined correction takes into account the overlapping part [16]. The radii of the WS spheres were obtained by requiring that the overlapping potential be the best possible approximation to the full potential, and were determined by an automatic procedure described in Ref. [16]. This overlap should not be too large because the error in the kinetic energy introduced by the combined correction is proportional to the 4th power of the relative sphere overlap. Interstitial spheres are needed because the structure of the compound under examination is not densely packed. The optimal positions and radii (r_{ES}) of these "empty spheres" (ES) were determined according to the method described in Ref. [16] and are specified in supplementary material.

The basis set included Al 3*s*, 3*p* and 3*d* orbitals, Ce 6*s*, 6*p*, 5*d* and 4*f* orbitals and Ni 4*s*, 4*p* and 3*d* orbitals. For the ES *s* and *p* orbitals or *s*, *p* and *d* orbitals were used depending on the size of the sphere. The Al 3*d* orbital, Ce 6*p* orbital and the ES *p* and *d* orbitals were treated by the Löwdin downfolding technique [13]. The **k**-space integrations were done by the tetrahedron method [17].

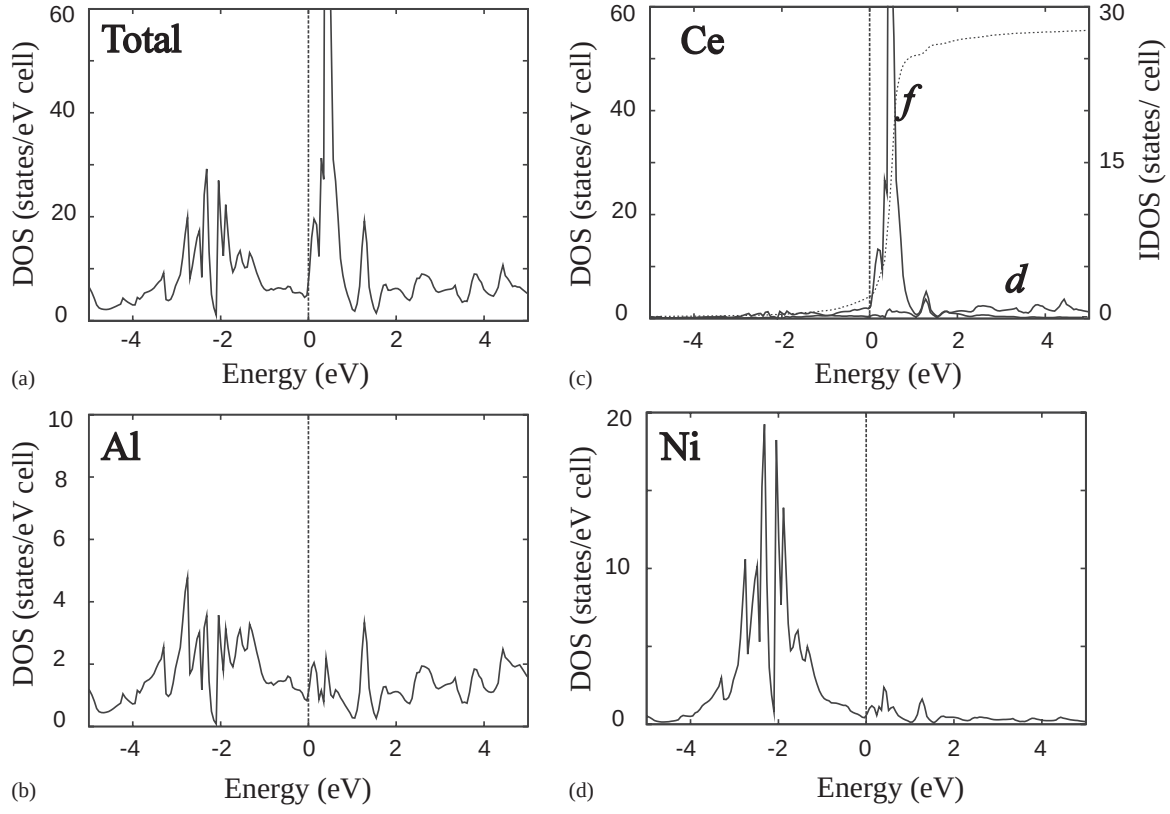

Fig. 8. (a) TDOS and different PDOS for $CeNiAl_4$, (b) Al PDOS, (c) Ce-*f* and Ce-*d* PDOS, and (d) Ni PDOS.

The self-consistent charge density was obtained using 32 irreducible **k**-points in the Brillouin zone both for the orthorhombic cell for $CeNiAl_4$ and the monoclinic cell for $Ce_4Ni_6Al_{23}$. The contribution of the nonspherical part of the charge density to the potential was neglected. Both nonspin-polarized and spin-polarized calculations were performed. The Fermi level was selected to be the energy reference.

5.2. *CeNiAl$_4$*

To our knowledge, electronic structure calculations have never been attempted on $CeNiAl_4$. Only X-ray spectroscopy experiments have been reported, which compare the electronic structure around the Fermi level of $CeNiAl_4$ and Ce_2NiAl_5 [7]. So, we have calculated the electronic structure of $CeNiAl_4$ as well. Not only will it complete the analysis and find a possible relation between the electronic structure and the physical behavior of this compound, this calculation could help to analyze the electronic structure of $Ce_4Ni_6Al_{23}$.

In Fig. 8 the total density of states (TDOS) and the partial density of states (PDOS) from each element obtained is shown for the $CeNiAl_4$ structure. According to Fig. 8, we notice that between -3 and -1 eV, the density of states (DOS) contribution is mostly from Ni-3*d* and Al-3*p* orbitals. The Ni-3*d* block is split symmetrically into two parts. There is a deep minimum in the DOS around -2 eV due to the symmetry of the local environment of this atom. Just above the Fermi level, we observe a huge peak from the Ce-4*f* orbitals, then the Ce-5*d* orbitals around 2 eV. However, careful examination of the Al-3*p* PDOS and Ni-3*d* PDOS indicates some contributions just above the Fermi level, which suggests some interactions between these orbitals and the Ce-4*f* orbitals. This is unusual considering that the Ce-4*f* orbitals are not often considered as involved in chemical bonding, but as localized states. These calculations confirm the existence of interactions between orbitals of the valence band with some Ce-4*f* orbitals which was suspected by the susceptibility measurements above 100 K.

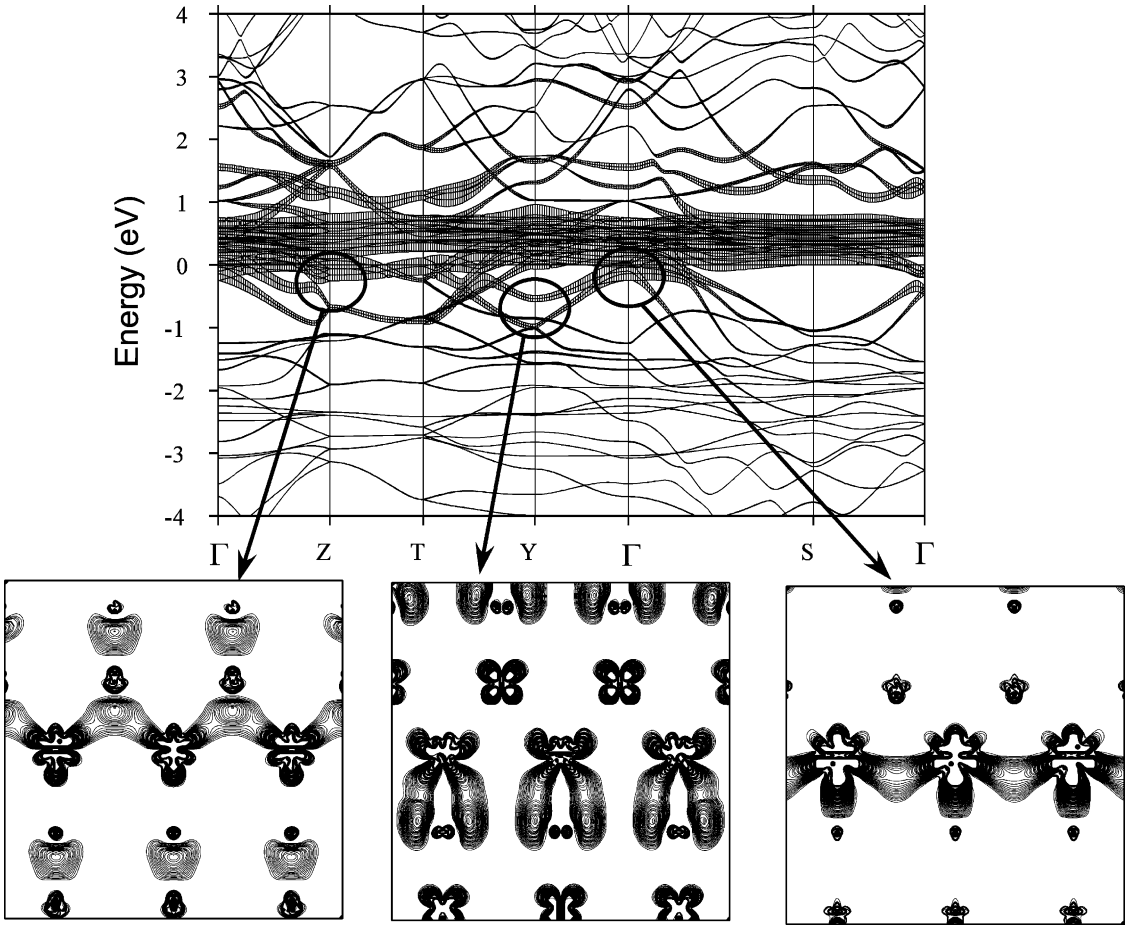

Fig. 9. Energy band dispersion of $CeNiAl_4$ with a fatband contribution for Ce-*f*. $\Gamma = (0,0,0)$, $Z = (0,0,1/2)$, $T = (0,1/2,1/2)$, $Y = (0,1/2,0)$, and $S = (1/2,1/2,0)$. Below, three electron density maps for some specials energies and special **k**-points (circles) are shown. These maps correspond to the (a,b) plane at $z = 1/4$.

The band structure of $CeNiAl_4$ is shown in Fig. 9 using a "fatband" representation for the Ce-4*f* orbitals (the amount of Ce-4*f* character in the band is represented by the width of the band). Most of the Ce-4*f* orbitals are localized at the Fermi level, which could explain the heavy fermion behavior. However, at some **k**-points we can see stabilization and destabilization of some bands with a Ce-4*f* character relative to the 4*f* reference energy (band center). Electron density calculations have been performed for three special **k**-points (Γ, Z and Y) on small energy windows including one or two bands for each point. The three plots presented in Fig. 9 show bonding interactions between Ce-4*f* orbitals either with other Ce-4*f* orbitals and/or Ni-3*d* and Al-3*p* orbitals. In the center of the square, which represents the (a,b) plane at $z = 1/4$, we recognize the shape of some Ce-4*f* orbitals. These three plots show only bonding interactions, which stabilize the bands. However, there are also orbitals in the conduction band that correspond to the antibonding cases. Moreover, only interactions in the (a,b) plane are shown in these plots, whereas the study of other bands for some other energy windows and some other **k**-points also shows interactions in the *c* direction.

5.3. $Ce_4Ni_6Al_{23}$

Fig. 10 shows the total DOS (TDOS) and the PDOS from each element obtained for the calculation on $Ce_4Ni_6Al_{23}$. These DOS are close to those obtained for $CeNiAl_4$, and agree well with the similarity observed for the different physical measurements. Previously, we noticed a deep minimum in the DOS for $CeNiAl_4$ around -2 eV. This minimum is still observed for $Ce_4Ni_6Al_{23}$ but it is less pronounced. The loss of symmetrical environments around Ni could be one reason.

To analyze the different interactions in $Ce_4Ni_6Al_{23}$, various crystal overlap Hamilton populations (COHPs [18]) have been examined for the main interatomic distances (Fig. 11). –COHPs of the Al–Ni, Ce–Ni and Al–Ce interactions show a crossing point between the bonding and antibonding states near the Fermi level, which is in agreement with the stability of the structure. Indeed, most of the bonding states are populated whereas antibonding states remain empty. This crossing is especially prominent for the Al–Ni interactions, which are the shortest distances in the structure. Similar COHP studies on $CeNiAl_4$ show similar results. These COHP results are consistent with recent investigations of "polar intermetallics" [19,20], and demonstrate that in the Ce–Ni–Al system, different structures may arise that will optimize bonding within the electronegative Ni–Al component.

Fig. 12 presents the energy dispersion of the bands for $Ce_4Ni_6Al_{23}$, with a fatband representation of the Ce-4*f* orbitals. As in $CeNiAl_4$, these valence orbitals

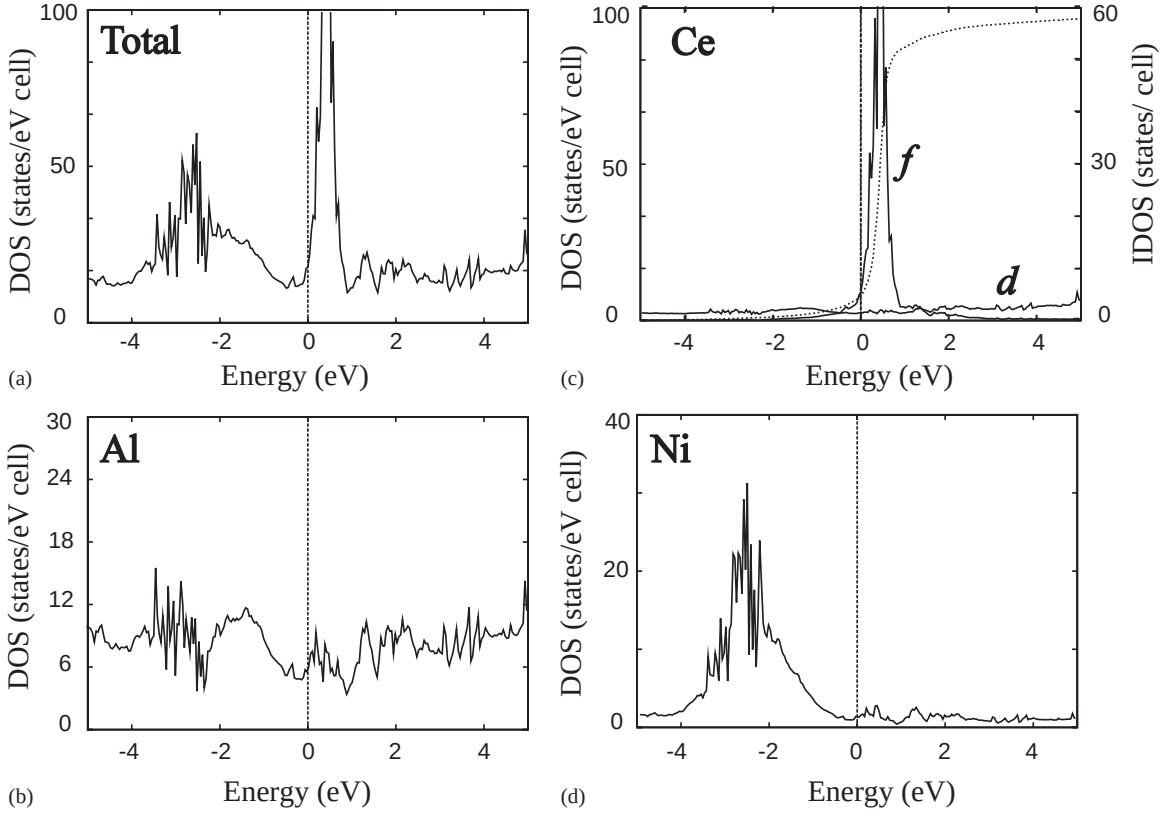

Fig. 10. (a) TDOS and different PDOS for $Ce_4Ni_6Al_{23}$, (b) Al PDOS, (c) Ce-*f* and Ce-*d* PDOS and (d) Ni PDOS.

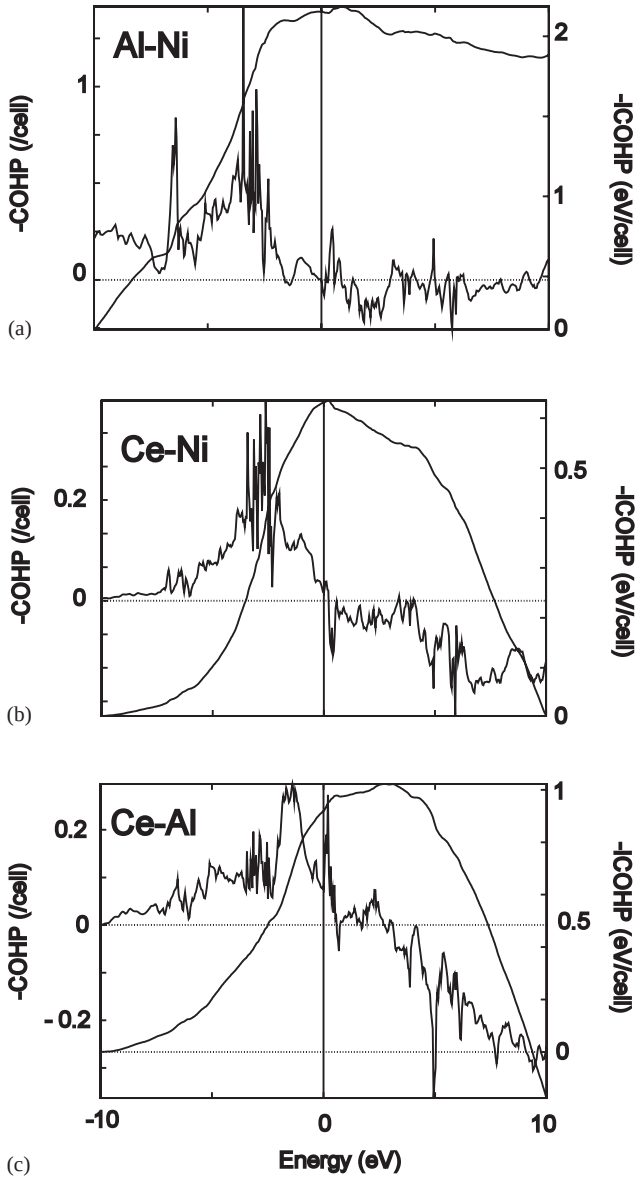

Fig. 11. COHP and integrated COHP (ICOHP) in $Ce_4Ni_6Al_{23}$ for (a) Al–Ni, (b) Ce–Ni and (c) Ce–Al short distances interactions.

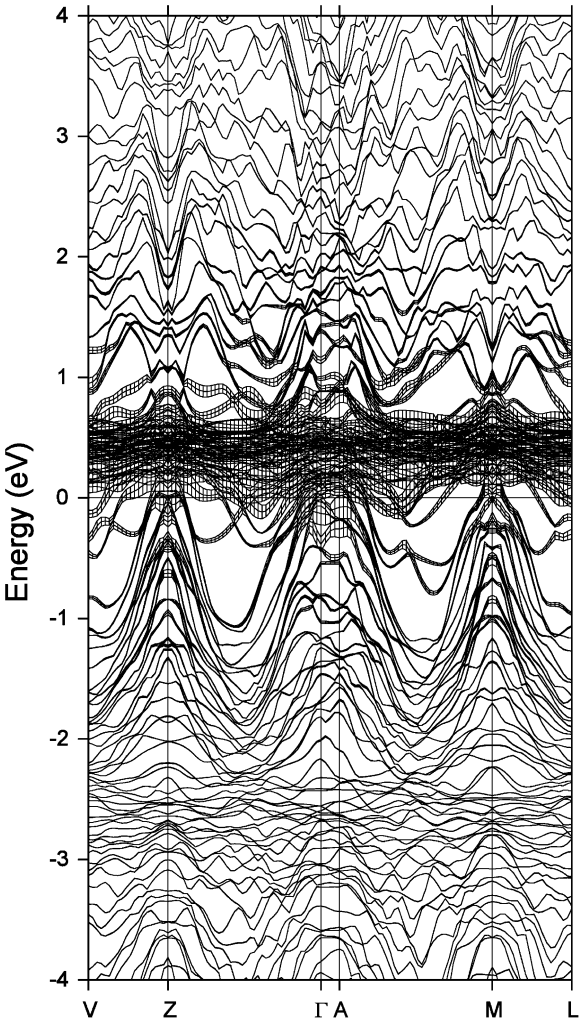

Fig. 12. Energy band dispersion of $Ce_4Ni_6Al_{23}$ with a fatband contribution for Ce-*f*. $V = (0, 1/4, 1/4)$, $\Gamma = (0, 0, 0)$, $Z = (0, 0, 1/2)$, $A = (1/2, 0, 0)$, $M = (1/2, 0, 1/2)$ and $L = (1/2, 1/4, 1/4)$.

participate in the bonding and antibonding interactions of the electronic structure. Some plots of the electronic density show identical pictures as presented in Fig. 10 for $CeNiAl_4$. Finally, along the *VZ* and *ML* directions, both parallel to $\mathbf{c}*$, there are large dispersions of some bands in the 2 eV range below the Fermi level. These dispersions are due to σ interactions along the *c* direction between Al-3*p*/Al-3*p* orbitals and Al-3*p*/Ni-3*d* orbitals. Similar dispersions exist for $CeNiAl_4$.

To summarize these results, the calculations show similarities between the electronic structures of $CeNiAl_4$ and $Ce_4Ni_6Al_{23}$ and, so, their analogous physical properties may be understood. Considering the proximity in the energy scale of Ce-4*f* orbitals, Ni-3*d* orbitals and Al-3*p* orbitals, some interactions between the Ce-4*f* orbitals and other valence orbitals are possible, which is in good agreement with the properties observed. Band structure calculations may explain the origin of the heavy fermion behavior in $CeNiAl_4$ and $Ce_4Ni_6Al_{23}$ by the presence of localized Ce-4*f* at the Fermi level. However, valence fluctuations as observed in $CeSn_3$ [21], which considers mixed Ce^{3+}/Ce^{4+} valence states at low temperature (under 100 K for $Ce_4Ni_6Al_{23}$), may also be at the origin of the temperature dependent magnetic susceptibility and resistance in these ternary compounds. Although the results of our electronic structure calculations strongly suggest the important role of the Ce-4*f* orbitals in these phenomena, further physical characterization of pure samples of $CeNiAl_4$ and $Ce_4Ni_6Al_{23}$ are needed to resolve this controversy. In addition, to explore the role of the 4*f* orbitals, we are examining the La–Ni–Al and Y–Ni–Al systems in the range of composition corresponding to $Ln_4Ni_6Al_{23}$. Preliminary results indicate that while $Y_4Ni_6Al_{23}$ exists

and is isostructural with $Ce_4Ni_6Al_{23}$, "$La_4Ni_6Al_{23}$" is not isostructural [22]. Physical and chemical characterization of these materials is currently underway.

Acknowledgments

This work was supported by the NSF DMR 99-81766. E. Benbow gratefully acknowledges the NSF through the Summer Research Program in Solid State Chemistry (DMR-0118443) for support. The authors are grateful to Warren Straszheim of the Materials Analysis Research Laboratory for performing energy-dispersive X-ray spectroscopy measurements on the samples. The authors also thank Sergey Bud'ko for the various physical property measurements on the samples and for useful discussions.

References

[1] A.E. Dwight, M.H. Mueller, R.A. Conner Jr., J.W. Downey, H. Knott, Trans. Metall. Soc. AIME 242 (1968) 2075.
[2] O.S. Zarechnyuk, T.I. Yanson, R.M. Rykhal, Izv. Akad. Nauk SSSR Met. 4 (1983) 192.
[3] (a) T. Mizushima, Y. Isikawa, A. Maeda, K. Oyabe, K. Mori, K. Sato, K. Kamigaki, J. Phys. Soc. Japan 60 (1991) 753.
(b) T. Mizushima, Y. Isikawa, K. Oyabe, K. Mori, J. Sakurai, Physica B 186 (1993) 457.
[4] Y. Isikawa, T. Mizushima, K. Oyabe, K. Mori, K. Sato, K. Kamigaki, J. Phys. Soc. Japan 60 (1991) 1869.
[5] Y. Isikawa, K. Mori, K. Kamigaki, T. Mizushima, K. Oyabe, S. Ueda, K. Sato, J. Magn. Magn. Mater. 108 (1992) 157.
[6] Y. Isikawa, T. Mizushima, J. Sakurai, K. Mori, A. Munoz, F. Givord, J.-X. Boucherle, J. Voiron, I.S. Oliveira, J. Flouquet, J. Phys. Soc. Japan 63 (1994) 2349.
[7] Y. Isikawa, H. Tagaki, A. Ishugiro, M. Yasumoto, T. Kuwai, T. Mizushima, J. Sakurai, A. Sawada, T. Komatsubara, K. Maezawa, H. Harima, J. Phys. Soc. Japan 68 (1999) 2802.
[8] T. Kashiwakura, T. Okane, S. Suzuki, S. Sato, M. Watanabe, A. Harasawa, T. Kinoshita, A. Kakizaki, T. Ishi, S. Nakai, Y. Isikawa, J. Phys. Soc. Japan 69 (2000) 3095.
[9] K.M. Poduska, F.J. DiSalvo, V. Petricek, J. Alloys Compd. 308 (2000) 64.
[10] STOE Software: Crystal Optimization for Numerical Absorption Correction, Stoe & Cie Gmbh, Darmstadt, Germany, 1996.
[11] V. Petricek, M. Dusek, jana2000: Programs for modulated and composite crystals, Institute of Physics, Praha, Czech Republic, 1998.
[12] A. Altomare, G. Cascarano, C. Giacovazzo, A. Guagliardi, A.G.G. Moliterni, M.C. Burla, G. Polidori, M. Camalli, R. Spagna, Sir97, A package for crystal structure solution by direct methods and refinement, Italy, 1997.
[13] (a) O.K. Andersen, Phys. Rev. B 12 (1975) 3060.
(b) O.K. Andersen, O. Jepsen, Phys. Rev. Lett. 53 (1984) 2571.
(c) O.K. Andersen, O. Jepsen, D. Glötzel, W.R.L. Lambrecht, in: F. Bassani, F. Fumi, M.P. Tosi (Eds.), Highlights of Condensed-Matter Theory, North-Holland, New York, 1985.
(d) O.K. Andersen, Phys. Rev. B 34 (1986) 2439.
[14] U. von Barth, L. Hedin, J. Phys. C 5 (1972) 1629.
[15] D. Koelling, B.N. Harmon, J. Phys. C 10 (1977) 3107.
[16] O. Jepsen, O.K. Andersen, Z. Phys. B 97 (1995) 645.
[17] P.E. Blöchl, O. Jepsen, O.K. Andersen, Phys. Rev. B 49 (1994) 16223.
[18] R. Dronskowski, P.E. Blöchl, J. Phys. Chem. 97 (1993) 8617.
[19] U. Häussermann, S. Amerioun, L. Eriksson, C.-S. Lee, G.J. Miller, J. Am. Chem. Soc. 124 (2002) 4371.
[20] G.J. Miller, C.-S. Lee, W. Choe, in: G. Meyer, D. Naumann, L. Wesemann (Eds.), Inorganic Chemistry Highlights, Wiley-VCH, Berlin, 2002.
[21] H. Harima, T. Kasuya, J. Magn. Mat. 52 (1985) 179.
[22] D. Gout, O. Gourdon, E. Benbow, G.J. Miller, to be published.